metals

MDPI

Article

Effect of Temperature on the Kinetics of Localized Plasticity Autowaves in Lüders Deformation

Vladimir I. Danilov, Dina V. Orlova *, Vadim V. Gorbatenko and Lidiya V. Danilova

Institute of Strength Physics and Materials Science, Siberian Branch, Russian Academy of Sciences, Tomsk 634055, Russia

* Correspondence: dvo@ispms.ru; Tel.: +7-3822-286-923

Abstract: The paper analyzes the elastoplastic transition in Fe–0.025 wt. % C at a temperature of 296–503 K and strain rate of $6.67 \cdot 10^{-6}$–$3.33 \cdot 10^{-3}$ s^{-1}. The analysis shows that the lower yield stress increases by a power law with increasing the strain rate, and that its rate sensitivity decreases linearly with increasing the test temperature. At temperatures lower than 393 K, the rate sensitivity of the lower yield stress is normal, and at 393–503 K, it is zero. In the range 393–503 K, the kinetics of the Lüders bands is changed from steady to discrete, and the higher the strain rate, the higher the temperature of this transition. Using the available data on the dynamics of dislocations and diffusion of interstitial impurities in the test alloy, it is demonstrated that the kinetics of Lüders bands are controlled by the effect of dynamic strain aging. If the arrest time of mobile dislocations t_w at barriers which are overcome via thermal activation is comparable with the precipitation time of interstitial atoms t_a at these dislocations, the motion of a Lüders band is discrete, and the band represents an excitation wave of localized plasticity; its refractory period is determined by the time of dynamic strain aging. If $t_a >> t_w$, the band moves monotonically and represents a switching autowave. The results of the analysis suggest that the effect of serrated yielding at the lower temperature boundary of blue brittleness can be suppressed by increasing the strain rate. When the arrest time of dislocations t_w decreases, the comparability of t_w and t_a is broken, and no excitation autowave is formed. The data reported in the paper can be used to develop warm rolling technologies for materials with a sharp elastoplastic transition.

Keywords: elastoplastic transition; lower yield stress; temperature; blue brittleness; serrated deformation; dynamic strain aging; localized plasticity autowaves

Citation: Danilov, V.I.; Orlova, D.V.; Gorbatenko, V.V.; Danilova, L.V. Effect of Temperature on the Kinetics of Localized Plasticity Autowaves in Lüders Deformation. *Metals* **2023**, *13*, 773. https://doi.org/10.3390/met13040773

Academic Editor: Ji Hoon Kim

Received: 27 February 2023
Revised: 4 April 2023
Accepted: 13 April 2023
Published: 15 April 2023

1. Introduction

The description of plastic deformation is one of the most complex problems associated with condensed matter. The significance of its fundamental and applied aspects is obvious and does not require any special proof. The theory of plastic deformation, being now an independent scientific discipline, is focused on the nonlinear response of condensed matter to external mechanical loads applied at different rates and under different thermodynamic conditions [1]. The behavior of plasticity is generally considered in the context of two mutually supplementary approaches. One of the approaches stems from mechanics [2], and the other from dislocation theories [3–6] intended to explain the physical mechanisms of plastic flow and the nonlinearity of its curve, which are unexplainable in terms of mechanics. The dislocation approach offers numerous specific deformation models, but it fails to offer a closed plasticity theory of solids. The problem is that microscopic plastic strain carriers, i.e., dislocations, are highly interacting objects, and their contribution to macroscopic deformation is not additive.

The idea of plastic flow as self-organization of an open thermodynamic system [7] provides the way of applying the thermodynamic theory of nonequilibrium systems or synergetics to deformed solids [8]. According to this theory, open nonlinear systems are prone

to various localization processes. Abundant research data point to several scales of plastic deformation [9–11]. Considered, as a rule, are three interrelated scales: the microscopic (dislocations), mesoscopic (dislocation ensembles), and macroscopic (specimen). Each scale of deformation has a characteristic correlation length over which the process develops. For the microscale, this length compares with the dislocation Burgers vector $b \approx 10^{-10}$ m.

For the mesoscale, it measures 10^{-6} m $\approx 10^{4}$ b. The mesoscale is related to dislocation ensembles which evolve as individual defects, rather than the individual dislocations, through a complex spontaneous process. This scale and respective plastic phenomena are the subject of physical mesomechanics pioneered by Panin [9].

For the macroscale, the characteristic correlation length ranges approximately from 10^{-3} to 10^{-1} m, which corresponds to the size of deformed specimens. On this scale, the plastic strain carriers are macrobands formed via macroscopic stress concentrator relaxation.

Localization processes during deformation are observed at all scale levels, including macroscopic ones. Among the outcomes of the concept of multiscale plastic deformation is the theory of localized plasticity autowaves [12–14], which generally represent dissipation structures in active matter and have their universal source in deformed solids. The theory suggests that any object under external load with no specific action consists of macroscopic regions of localized plastic flow ordered in space and time. Within the framework of this theory, a deformable solid is a universal generator of various autowave modes of localized plasticity [12]. According to the rule of correspondence established in experiments (mostly for polycrystals with dislocation mechanisms of plastic flow), the mode of an autowave is determined by the hardening law active at a given stage of stress–strain curves [13].

Although the autowave concept of plastic flow is widely recognized by theoreticians [15–17] and experimenters [18–21], there are several key points in the concept that remain open. One of these points concerns the transition from homogeneous elastic deformation to localized plastic flow. Obviously, it is this transition that activates autowave mechanisms and gives rise to various autowave modes of localized plasticity.

The key point in the autowave concept of plastic deformation concerns the elastoplastic transition that activates autowave mechanisms, i.e., gives rise to various autowave modes of localized plasticity. A striking example of this type of transition is the Lüders deformation in iron and its low-carbon alloys. After nucleation at a sharp yield point at room temperature, the Lüders band develops via the formation and monotonic motion of its fronts. Such fronts cover the working specimen space once, annihilate on meeting, and have other attributes of switching autowaves which allow the use of this autowave mode for describing the Lüders deformation [14].

However, in the range of normal strain rates and temperatures 423–510 K, the stress is pulsating and the development of Lüders bands is unsteady [22,23]. This range of temperatures and strain rates is the range of blue brittleness of mild steels. In technological terms, blue brittleness is undesirable. In particular, its range falls on the temperatures and strains rates at which mild steels are exposed to warm forming, wherein their homogeneous plastic deformation is important [24]. For this reason, there is unceasing interest in the Lüders deformation under the above temperature–rate conditions [25–29]. In particular, two questions in this context remain open: how Lüders bands move under such conditions, and whether they can be considered switching autowaves. Presented below is an analysis of the effect of temperature and strain rate on the Lüders deformation in mild steels.

2. Materials and Methods

The traditional material for the study of Lüders deformation, as mentioned above, is mild steel [20,25,26,28]. In this work, studies were carried out on samples of ARMCO iron, the chemical composition of which is presented in weight percent in Table 1 below. A hot-rolled plate of thickness 1.5 mm was laser-cut to obtain dog bone-shaped specimens with a gage section of 50 × 10 mm^2. To provide more uniform stresses and structure, the specimens were preliminarily annealed in a vacuum furnace until recrystallization (1233 K, 1 h) and then cooled with a furnace to room temperature.

Table 1. Chemical composition of ARMCO iron.

Elements	C	Si	Cu	Mn	S	P	Fe
wt. %	0.025	0.05	0.05	0.035	0.01	0.01	balance

The prepared specimens were exposed to uniaxial tension on a Walter + Bai AG LFM-125 testing machine at a constant rate. The crosshead rate was varied from 0.02 to 10 mm/min, which corresponds to strain rates from $6.67 \cdot 10^{-6}$ s^{-1} to $3.33 \cdot 10^{-3}$ s^{-1} for the specimen size used, and the test temperature was varied from 296 to 503 K. The furnace (Walter + Bai STE-12H) ensured independent temperature control in three zones. The specimen temperature was measured with three type K thermocouples located along the specimen axis at 20 mm from each other. First, the specimens were heated to the desired temperature at the same operating temperature specified for all three zones. Once the furnace reached its operating mode, a minimum or a desired temperature gradient along the specimen length was set by varying the temperature in each zone of the furnace.

To study the kinetics of macroscopic strain localization sites, successive digital images of the tensile specimens were recorded. To form a speckle structure, the specimens were illuminated by coherent light from a semiconductor laser (635 nm, 15.0 mW). Such a method of speckle structure formation does not require any addition specimen surface preparation. The images of the specimens were recorded using a Point Grey FL3-GE-50S5M-C digital video camera (resolution 2448 × 2048 px) with a rate of 2 to 25 frames per second, depending the applied strain rate. The camera with a Kowa LM50JC10M lens was located at 0.3 m from the specimens, which provided a resolution of 20.4 μm/pixel. The image sequence was processed by the digital image correlation (DIC) method [30] and digital statistical speckle photography [31–33]. In the latter method, a sampling with a specified length is formed for each point of a digital image to characterize the time dependence of its brightness, and the variance and expectation are calculated. Their ratios are used to image strain localization zones. This method does not require any tedious calculations and allows one to identify in situ the regions in which strains are localized at a given increment of the total specimen elongation. Besides, the method of digital statistical speckle photography, compared to the DIC method, increases the spatial and time resolution by two orders of magnitude, as no area averaging is needed, and the time window for two adjacent images can be decreased to a minimum. The shortcoming of the method is that it is insensitive to weakly localized and smeared fronts, which are just well identified by the DIC method. The recorded image sequence was processed by the DIC method successively for each image pair spaced by a certain time interval. The interval was chosen according to the elongation rate so that the total specimen elongation within the given interval was no greater than 50 μm. For calculations, subsets of size 32 × 32 pixels were used. The method of calculation was standard iteration, which allows estimations of displacements with an accuracy of no worse than 0.1 pixel, i.e., 2 μm, at the video camera resolution mentioned above.

From the data arrays obtained, chronograms were constructed [14,25], allowing us to identify the nuclei of Lüders bands and to determine the kinetic characteristics of their fronts.

3. Results and Discussion

The form of loading diagrams of low-carbon steels is influenced by the test temperature and strain rate [22]. At room and lower temperatures, they contain a sharp yield point, a smooth yield plateau, and a gradual hardening stage almost with any strain rate (Figure 1a). However, increasing the temperature to those of blue brittleness can radically change their form. At a temperature of 393 K and strain rate of $6.67 \cdot 10^{-5}$ s^{-1}, there are stress jumps at the yield plateau and serrated yielding at the hardening stage (Figure 1b). At a temperature of 423 K and same strain rate, the whole plateau is serrated (Figure 1c). However, at a strain rate of $2.67 \cdot 10^{-4}$ s^{-1} and same temperature, the plateau is smooth, though serrated yielding is present at the hardening stage (Figure 1d). However, if at this loading rate the test temperature is increased to 463 K, the yield plateau will be serrated (Figure 1e). Finally,

at 503 K and $6.67 \cdot 10^{-5}$ s^{-1}, neither the hardening stage nor the plateau reveal serrated yielding, and the plateau degenerates (Figure 1f). Thus, in the temperature range of blue brittleness at relatively high rates, one can observe a sharp yield point and a smooth plateau similar to those appearing at room temperature.

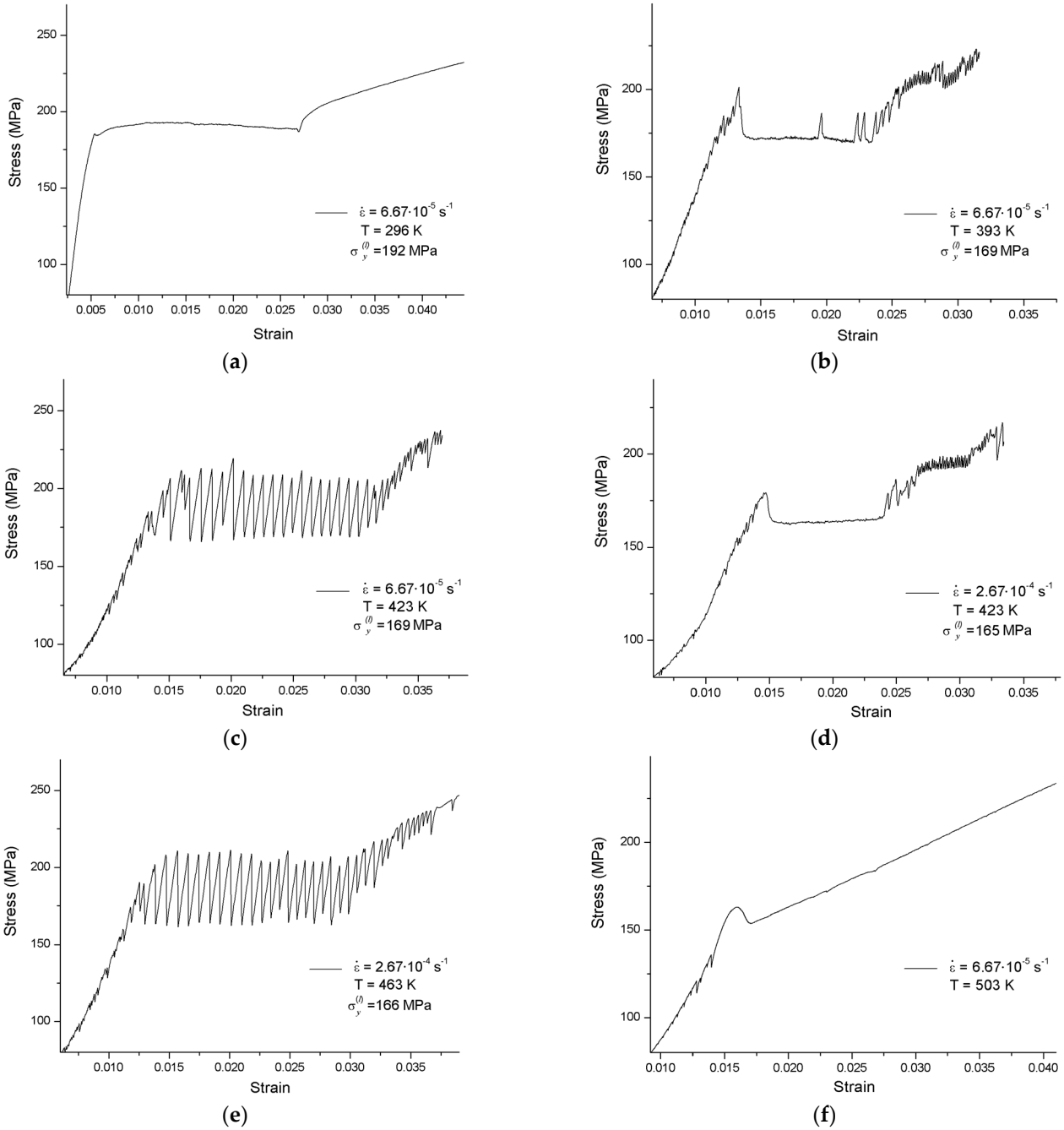

Figure 1. Loading curve at T = 296 K, $\dot{\varepsilon} = 6.67 \cdot 10^{-5}$ s^{-1} (**a**); T = 393 K, $\dot{\varepsilon} = 6.67 \cdot 10^{-5}$ s^{-1} (**b**); T = 423 K, $\dot{\varepsilon} = 6.67 \cdot 10^{-5}$ s^{-1} (**c**); T = 423 K, $\dot{\varepsilon} = 2.67 \cdot 10^{-4}$ s^{-1} (**d**); T = 463 K, $\dot{\varepsilon} = 2.67 \cdot 10^{-4}$ s^{-1} (**e**); T = 503 K, $\dot{\varepsilon} = 6.67 \cdot 10^{-5}$ s^{-1} (**f**).

The temperature and the rate should also influence the stress corresponding to the yield plateau, i.e., the lower yield stress $\sigma_y^{(l)}$. It can be seen from Figure 2a that in the range from room temperature to 393 K, where the plateau is smooth at any rate, the lower yield stress $\sigma_y^{(l)}$ increases nonlinearly with increasing the strain rate. Increasing the temperature decreases $\sigma_y^{(l)}$ irrespective of the rate.

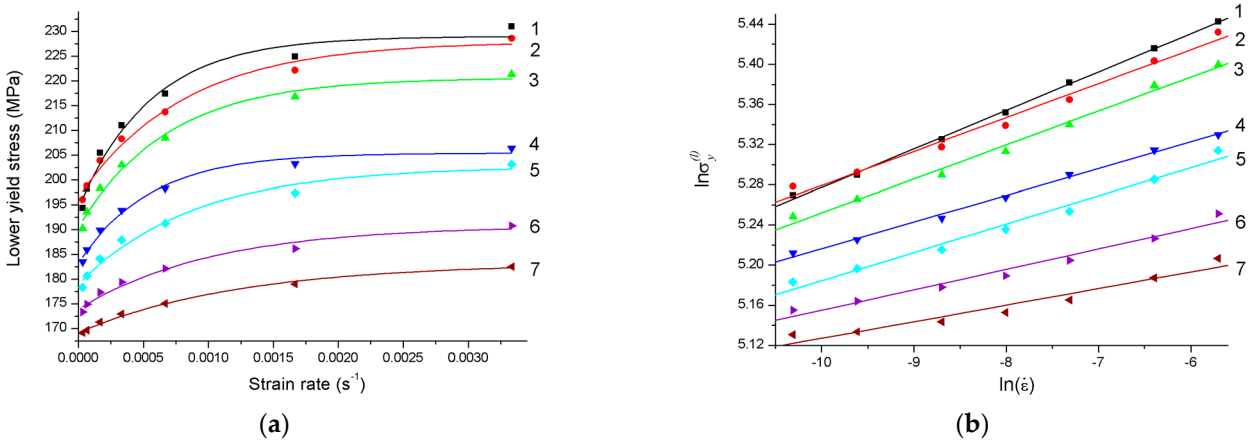

Figure 2. Rate dependences of lower yield stress at 296 (1), 313 (2), 323 (3), 333 (4), 343 (5), 373 (6), and 393 K (7) (**a**); the same in logarithmic coordinates (**b**).

In logarithmic coordinates, the rate dependences (Figure 2a) become linear (Figure 2b), and hence they can be interpolated by power functions of the form:

$$\sigma_y^{(l)} = \sigma_0 \dot{\varepsilon}_n^m \quad (1)$$

where $\dot{\varepsilon}_n = \dot{\varepsilon} t_{ph}$ is the relative tension rate normalized to the velocity of sound in the material with t_{ph} for the time of sound wave propagation in it, $\dot{\varepsilon} = V_{mach} l_0^{-1}$ with V_{mach} for the absolute tension rate and l_0 for the specimen gage section length, and σ_0 is a constant with a stress dimension. According to [34], such a power dependence follows from the equation of mechanical state and balance of mobile and immobile dislocation densities in a deformed solid. The exponent m is interpreted as the rate sensitivity index. In the study presented, this was determined for all test temperatures from the slope of the straight lines in Figure 2b. In this operation, the constant σ_0 is not used, and therefore its numerical value was not determined.

As can be seen from Figure 3, increasing the temperature linearly decreases the index m. Extrapolation of that linear function to zero gives a temperature of 503 K. This suggests that the lower yield stress is rate-insensitive at above 503 K. Actually, the situation is more intricate. According to [22], the lower bound of transition from steady to discrete Lüders bands is 435 K. However, as shown in Figure 1, the lower the strain rate, the lower the temperature of this bound. For example, at 393 K, the yield plateau reveals serrations if $\dot{\varepsilon} \leq 6.67 \cdot 10^{-5}$ s^{-1}; if the tension rate is higher than the above value, the plateau is smooth. At a test temperature of 423 K, there are no serrations observed at tensile rate $\dot{\varepsilon} \geq 2.67 \cdot 10^{-4}$ s^{-1}. At 463 K, the plateau is serrated irrespective of the tension rate from $6.67 \cdot 10^{-6}$ s^{-1} to $4 \cdot 10^{-4}$ s^{-1}. It should be noted that the lower level of stresses in a jump depends neither on the strain rate nor on the test temperature at 393–503 K, and measures 168 ± 4 MPa. Likely, this value can be taken as the lower yield stress for serrated plateaus. Thus, in the temperature–rate range indicated, the lower yield stress becomes insensitive to both the loading rate and the test temperature. It should be emphasized that this occurs at temperatures much lower than those suggested by the diagram in Figure 3.

From 503 K upward, there is no serrated yielding if $\dot{\varepsilon} \leq 6.67 \cdot 10^{-5}$ s^{-1}, such that the plateau degenerates and the stress–strain curve becomes close to its normal parabolic form.

Near the critical transition temperature at respective strain rates, part of the plateau can be smooth and the other can be serrated (Figure 4a,b). It should be emphasized that the minimum stress in yield drops coincides with the stress in the smooth part of the plateau, and that the rate dependence of this stress for respective temperatures is described by expression (1). This confirms the fact that the rate sensitivity of the lower yield stress under serrated deformation conditions does disappear.

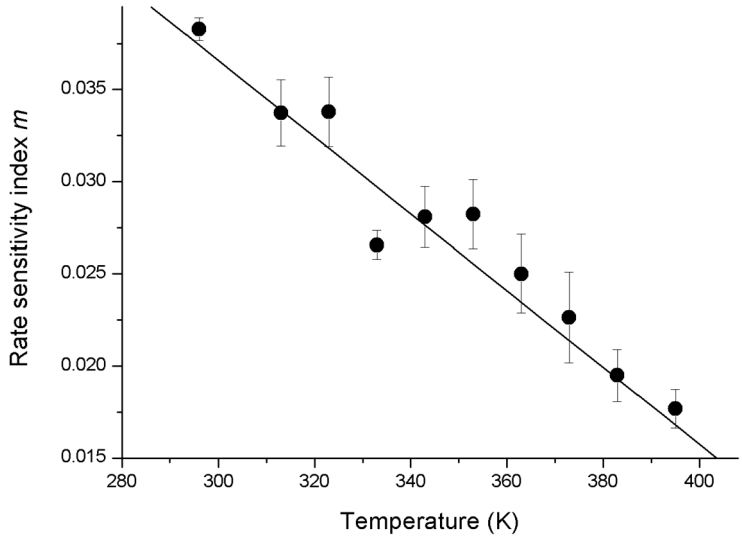

Figure 3. Dependence of the rate sensitivity index of the lower yield point on the test temperature.

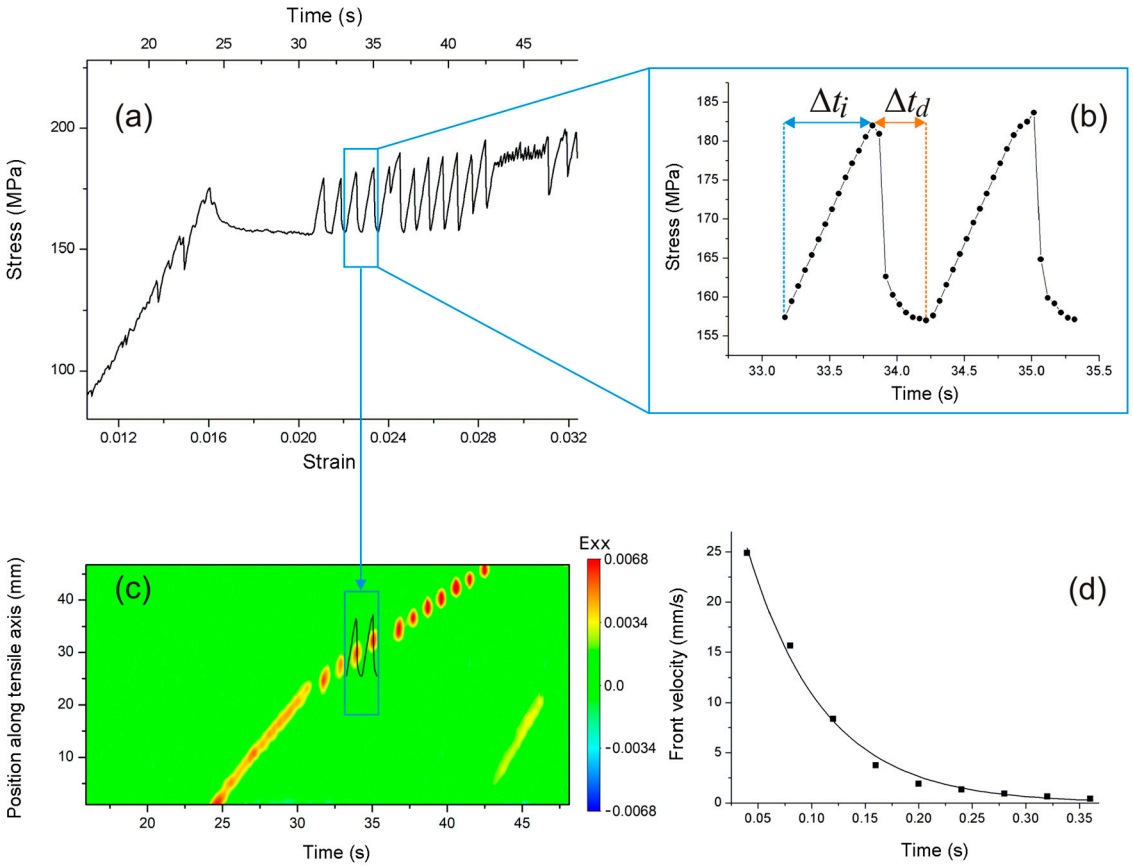

Figure 4. Yield plateau (**a**,**b**), Lüders front motion (**c**), front velocity (**d**) at temperature gradient 421–458 K along specimen length for tension rate $\dot{\varepsilon} = 6.67 \cdot 10^{-4}$ s^{-1}

If a single Lüders band develops near the grip of a testing machine, the deformation is localized at its front (the mobile band boundary). The motion of this front can be visualized from chronograms. As has been shown [14,22], the front velocity for a smooth yield plateau is constant, and is related to the strain rate as follows:

$$V_{mach} = \varepsilon_{pl} V_f \quad (2)$$

where ε_{pl} is the specimen strain which is accumulated at the yield plateau and is equal at any time point to the amplitude of strains localized at the front.

In certain Al alloys, the yield plateau can be both smooth and serrated [35–38]. As has been shown on the example of Al–5% Mg (Russian grade AMg5 or Al alloy 1550) by the method of digital speckle photography [38], the kinetics of strain fronts at the serrated plateau are such that they move only on the intervals of stress drop. The same is observed in the case considered.

Figure 4c shows the chronogram of the Lüders front motion for the case in Figure 4a. It is seen that the front changes its motion from continuous to discrete when deforming-stress fluctuations appear. The chronogram also suggests that the velocity of its continuous motion is higher than the average velocity of its discrete motion in a ratio of 1.75:1. Such a difference is likely because the front in serrated yielding moves not at a constant, but at an exponentially decreasing stress when its velocity also decreases exponentially (Figure 4d). At $\dot{\varepsilon} = 6.67 \cdot 10^{-4}$ s^{-1}, the intervals of stress drop and rise measure, respectively, at $\Delta t_d = 390$ ms and $\Delta t_i = 660$ ms (Figure 4b). Clearly, the average velocity of discrete front motion under such conditions cannot be equal to the front velocity at a constant stress under steady conditions.

Let us consider what causes the strain localization fronts to change their kinetics of motion under the action of temperature. The effect of serrated yielding arises when the normal strain rate dependence of the hardening coefficient becomes negative [39]. The results presented in Figure 2a,b show that at 296–393 K, the lower yield stress increases with the increasing rate. The rate sensitivity is normal. At above 393 K but below 503 K, the lower yield stress $\sigma_y^{(l)}$ does not depend on the rate and temperature (Figure 1b–e). At the same interval, the behavior of the material reveals an anomalous jump-like motion of the strain fronts.

The physical mechanism of this phenomenon can be analyzed by comparing the Lüders and the Portevin–Le Chatelier types of flow within the autowave concept of plastic deformation. If the front of a Lüders band is a switching autowave, the deformed object should be a bistable active material which transforms at the front from its metastable elastic to its stable plastic state. Such a transition in a bistable material is possible only once.

However, the same transition from elastic to plastic deformation happens at the fronts of Portevin–Le Chatelier bands, which can repeatedly pass through an object [29,38]. Such bands arise in excitable active materials and are interpreted as excitation autowaves [40]. Excitable active materials, unlike bistable ones, have the property of recovery characterized by the period of refractory, i.e., by the time for which they remain indifferent to external actions and realize only a certain sequence of internally specified transitions. However, if the period of refractory is much longer than the time of observation of a system, no recovery occurs, and the system can no longer be considered excitable. Hence, any bistable material is formally an excitable medium with an infinite refractory period. Let us ascertain what can be interpreted as the refractory period in the case considered.

The effect of blue brittleness in diluted interstitial solid solutions based on bcc iron, similar to the Portevin–Le Chatelier effect in aluminum alloys, is governed by dynamic strain aging [23,37,40,41]. On the microscale, this aging is controlled by two processes: a thermally activated dislocation motion with forest dislocation barriers, and additional trapping of dislocations via diffusion precipitation of interstitial atoms at them. Neglecting the time of dislocation motion between the barriers, the first process is characterized by the dislocation arrest (waiting) time at a barrier t_w, and the second by the time of strain aging, i.e., the time of impurity atom diffusion to retarded dislocations, t_a. If the strain rate is high and the test temperature is rather low, the time t_w is insufficient for impurity atoms to reach retarded dislocations, such that the latter, once divorced from the impurity cloud, continue their free motion. At low strain rates and high temperatures, a cloud is formed by impurity atoms within the time t_w, and such a cloud and dislocations move together. In both cases, increasing the strain rate increases the resistance to plastic flow, i.e., the rate sensitivity is normal. However, an intermediate interval of rates (temperatures)

exists, at which the two characteristic times are comparable. In this case, not all retarded dislocations gain an impurity atmosphere, and those that remain free rapidly multiply with the formation of a front similar to Lüders fronts, and anomalous rate sensitivity arises [39]. Reasoning from the above, the period of refractory during the propagation of a strain front is the time of dynamic strain aging, t_a. If this time is comparable with t_w, the deformed object will represent an excitable system, and the strain front an excitation autowave of localized plastic deformation. The motion of this front is discrete.

Let us estimate the ratio of t_w and t_a at 296 K (room temperature) and 393 K. These temperatures were chosen from the following reasoning. At 296 K irrespective of the strain rate, the yield plateau is smooth, the motion of strain fronts is monotonic, and the rate sensitivity is normal. At 393 K with $\dot{\varepsilon} = 3.33 \cdot 10^{-5}$ s^{-1}, the yield plateau reveals stress jumps, the motion of strain fronts is discrete, and the rate sensitivity is absent.

According to the theory of thermally activated dislocation motion, the waiting time at a barrier depends on the densities of mobile dislocations ρ_m and forest dislocations ρ_f. It is inversely proportional to the strain rate $\dot{\varepsilon}$, and can be expressed as [41]

$$t_w = \frac{\Lambda \rho_m b}{\dot{\varepsilon}} = \frac{\rho_m b}{\dot{\varepsilon}\left(\rho_f\right)^{1/2}}. \quad (3)$$

Here, $\Lambda = \left(\rho_f\right)^{-1/2}$ is the average spacing of barriers (forest dislocations), and b is the Burgers vector of dislocations for bcc iron.

The time of dynamic aging is determined by the diffusion of interstitial impurity atoms and by the impurity atom–dislocation binding energy U_m [23]:

$$t_a = \left(\frac{C_1}{\alpha C_0}\right)^{3/2} \frac{kTb^2}{3DU_m} \quad (4)$$

where C_1 is the impurity concentration which falls on the line of a dislocation and is required for its arrest, C_0 is the average impurity concentration in the alloy, and k is Boltzmann's constant. It is accepted [23] that $C_1 = 1$ and $\alpha = \pi$. According to [23,42], the impurity diffusion coefficient D is expressed as

$$D = D_0 exp\left(-\frac{\Delta H}{RT}\right) \quad (5)$$

where D_0 is the pre-exponential factor, ΔH is the diffusion activation energy, and R is the universal gas constant. Combining Equations (4) and (5) allows us to express t_a as

$$t_a = \left(\frac{1}{\pi C_0}\right)^{3/2} \frac{kTb^2}{3D_0U_m} exp\left(\frac{\Delta H}{RT}\right) \quad (6)$$

Let the main interstitial impurity be carbon, whose average concentration in ARMCO iron is $C_0 = 2.5 \cdot 10^{-4}$. According to [23,42], ΔH = 20,100 cal/mol, $D_0 = 0.02$ cm^2/s, $U_m = 0.55$ eV, and $b = 2.48 \cdot 10^{-8}$ cm. According to table values, $R = 2$ cal/mol, $k = 0.8625 \cdot 10^{-4}$ eV/K. Then, $t_a \approx 1.2 \cdot 10^4$ s at $T = 296$ K. If, following [23], $\rho_m = \rho_f = 10^8$ cm^{-2}, the waiting time given by Equation (3) for $\dot{\varepsilon} = 3.33 \cdot 10^{-5}$ s^{-1} is $t_w \approx 6$ s. It can be seen that at room temperature, $t_a >> t_w$, and no repeated dislocation arrest by impurities takes place. Hence, the initial material state cannot be recovered and the front should move monotonically, representing a switching autowave.

At T = 393 K, according to (6), $t_a \approx 4$, and hence, it is close to t_w. Therefore, the recovery of impurity atmospheres is possible and the front should move discretely, representing an excitation autowave. The above estimates confirm the experimental data.

At temperatures above 393 K, the time of strain aging t_a decreases rapidly, such that the comparability of t_a and t_w will hold at increasingly higher strain rates; that is, increasingly higher strain rates will provide the formation of an excitable medium, switching-to-excitation autowave transformation, and discrete strain front motion. However, at 503 K, $t_a \approx 0.02$ s. This aging time is much shorter than the waiting time $t_w \approx 6$ s at the strain rate $\dot{\varepsilon} = 3.33 \cdot 10^{-5}$ s^{-1} considered; hence, the motion of dislocations is always accompanied by impurity atmospheres. Under such conditions, according to [39,41], the rate sensitivity should be normal, and any serrated deformation should be absent. The results of the study presented confirm that this is true (see Figure 1f).

4. Conclusions

The results of the study on the elastoplastic transition in Fe–0.025 wt. % C at a temperature of 296–503 K and strain rate of $6.67 \cdot 10^{-6}$–$3.33 \cdot 10^{-3}$ s^{-1} allow for the following conclusions to be drawn:

1. At 296–393 K, the lower yield stress increases by a power law with an increase in the strain rate; that is, the rate sensitivity is normal. At these temperatures, the rate sensitivity index is lower than one.
2. As the temperature is increased, the rate sensitivity index decreases linearly and becomes equal to zero at above 393 K. The normal rate sensitivity of the lower yield stress disappears.
3. At 393–503 K, the motion of Lüders bands is changed from steady to discrete. The higher the strain rate, the higher the temperature of transition to serrated Lüders deformation.
4. The kinetics of Lüders fronts are controlled by the times t_w and t_a, being, respectively, the arrest time of dislocations at barriers which are overcome via thermal activation (effect of dynamic strain aging) and the time of carbon impurity precipitation at these dislocations. The motion of strain fronts becomes discrete under those temperature-rate conditions with which t_w and t_a are comparable, and the rate sensitivity of the lower yield stress is absent.
5. When the motion of a strain front is discrete, the front represents an excitation autowave of localized plasticity whose refractory period is determined by the time of dynamic strain aging t_a. At temperatures lower than 393 K, when $t_a >> t_w$, the front moves monotonically and represents a switching autowave of localized plasticity.
6. At temperatures above 503 K, when $t_w \gg t_a$, the yield plateau degenerates and the normal rate sensitivity is recovered.

In summary, it can be stated that the effect of serrated yielding at the lower temperature boundary of blue brittleness can be suppressed by increasing the strain rate. This is possible due to the decrease in the arrest time of dislocations at barriers when the comparability of t_w and t_a is violated. In this case, no excitable medium is formed and no excitation autowave is generated. The established mechanisms can be used to develop warm rolling technologies for mild steels and other materials with a sharp elastoplastic transition.

Author Contributions: Conceptualization, writing—original draft preparation, V.I.D.; validation, formal analysis, investigation, V.I.D., D.V.O., V.V.G. and L.V.D.; writing—review and editing, methodology, software, V.V.G. All authors have read and agreed to the published version of the manuscript.

Funding: The work was supported by RSF grant No. 22-29-00171, https//rscf.ru/project/22-29-00171/(accessed on 21 December 2021).

Institutional Review Board Statement: Not applicable.

Informed Consent Statement: Not applicable.

Data Availability Statement: Not applicable.

Conflicts of Interest: The authors declare no conflict of interest.

References

1. Bell, F.G. *The Experimental Foundations of Solid Mechanics*; Springer: Berlin/Heidelberg, Germany, 1973; p. 825.
2. Rabotnov, Y.N. *Elements of Lineal Mechanics of Solids*; Nauka: Moscow, Russia, 1977; p. 384. (In Russian)
3. Kelly, A.; Groves, G.W. *Crystallography and Crystals Defects*; Longman: London, UK, 1970; p. 428.
4. Cottrell, A.H. *Dislocation and Plastic Flow in Crystals*; Oxford University Press: New York, NY, USA, 1953; p. 223.
5. Messerschmidt, U. *Dislocation Dynamics during Plastic Deformation*; Springer: Berlin, Germany, 2010. [CrossRef]
6. Hull, D.; Bacon, D.J. *Introduction in Dislocations*; Elsevier: Oxford, UK, 2011; p. 272.
7. Seeger, A.; Frank, W. *Nonlinear Phenomena in Materials Science*; Trans Tech Publications: New York, NY, USA, 1988; pp. 125–137.
8. Scott, A. *Nonlinear Science. Emergence and Dynamics of Coherent Structures*; Oxford University Press: Oxford, UK, 2003; p. 504.
9. Panin, V.E. Dynamic gauge theory of waves in elastoplastic media. In *Physical Mesomechanics of Heterogeneous Media and Computer-Aided Design of Materials*; Panin, V.E., Ed.; Cambridge International Science Publishing Ltd.: Cambridge, UK, 1998; pp. 97–117.
10. Panin, V.E.; Egorushkin, V.E. Basic physical mesomechanics of plastic deformation and fracture of solids as hierarchically organized nonlinear systems. *Phys. Mesomech.* **2015**, *18*, 377–390. [CrossRef]
11. Ohashi, T.; Kawamukai, M.; Zbib, H.M. A multiscale approach for modeling scale-dependent yield stressing polycrystalline metals, *Int. J. Plast.* **2007**, *23*, 897–914. [CrossRef]
12. Zuev, L.B. Using a crystal as a universal generator of localized plastic flow autowaves. *Bull. Russ. Acad. Sci. Phys.* **2014**, *78*, 957–964. [CrossRef]
13. Zuev, L.B.; Barannikova, S.A.; Danilov, V.I.; Gorbatenko, V.V. Plasticity: From crystal lattice to macroscopic phenomena. *Prog. Phys. Met.* **2021**, *22*, 3–57. [CrossRef]
14. Danilov, V.I.; Gorbatenko, V.V.; Zuev, L.B.; Orlova, D.V.; Danilova, L.V. Lüders deformation of low-carbon steel. *Steel Transl.* **2017**, *47*, 662–668. [CrossRef]
15. Tsagrakis, I.; Aifantis, C. On the effect of strain gradient on adiabatic shear banding. *Metall. Mater. Trans. A* **2015**, *46*, 44–59. [CrossRef]
16. Zaiser, M.; Aifantis, E.C. Randomness and slip avalanches in gradient plasticity. *Int. J. Plast.* **2006**, *22*, 1432–1455. [CrossRef]
17. Aifantis, E.C. Gradient material mechanics: Perspectives and Prospects. *Acta Mech.* **2014**, *225*, 999–1012. [CrossRef]
18. Shibkov, A.A.; Zolotov, A.E.; Gasanov, M.F.; Denisov, A.A.; Koltsov, R.Y.; Kochegarov, S.S. Nonlinear dynamics of an individual Portevin—Le Chatelier deformation bands. *Phys. Solid State* **2022**, *64*, 1583–1593. [CrossRef]
19. Asharia, A.; Beaudoin, A.; Miller, R. New perspectives in plasticity Theory: Dislocation nucleation, waves, and partial continuaty of plastic strain rate. *Math. Mech. Solids* **2008**, *13*, 292–315. [CrossRef]
20. Tretyakov, M.P.; Wildemann, V.E.; Tretyakova, T.V.; Safronov, S.A. Computational and experimental study of strain localization processes on the postcritical stage of deformation. *Proced. Struct. Integr.* **2021**, *33*, 871–877. [CrossRef]
21. Borg, U. Strain gradient crystal plasticity effects on flow localization. *Int. J. Plast.* **2007**, *23*, 1400–1416. [CrossRef]
22. Hall, E.O. *Yield Point Phenomena in Metals and Alloys*; Plenum Press: New York, NY, USA, 1970; p. 296.
23. Fridel, J. *Dislocations*; Pergamon Press: New York, NY, USA, 1964; p. 491.
24. Jacobs, T.R.; Matlock, D.K.; Findley, K.O. Characterization of localized plastic deformation behaviors associated with dynamic strain aging in pipeline steels using digital image correlation. *Int. J. Plast.* **2019**, *123*, 70–85. [CrossRef]
25. Sun, H.B.; Yoshida, F.; Ohmori, M.; Ma, X. Effect of strain rate on Lüders band propagating velocity and Lüders strain forannealed mild steel under uniaxial tension. *Mater. Lett.* **2003**, *57*, 4535–4539. [CrossRef]
26. Plekhov, O.A.; Naimark, O.B.; Saintier, N.; Palin-Luc, T. Elastic-plastic transition in iron: Structural and thermodynamic features. *Tech. Phys.* **2009**, *54*, 1141–1146. [CrossRef]
27. Liu, W.; Lian, J. Stress-state dependence of dynamic strain aging: Thermal hardening and blue brittleness. *Int. J. Miner. Metall. Mater.* **2021**, *28*, 854–866. [CrossRef]
28. Prokhorov, A.; Vshivkov, A.; Plekhov, O.; Kashaev, N.; Fomin, F.; Ozerov, M.; Zherebtsov, S. The effect of LSP on the structure evolution and self-heating of ARMCO-iron under cyclic loading. *Metals* **2021**, *11*, 1198. [CrossRef]
29. Varanasi, R.S.; Zaefferer, S.; Sun, B.; Ponge, D. Localized deformation inside the Lüders front of a medium manganese steel *J. Mater. Sci. Eng. A* **2021**, *824*, 141816. [CrossRef]
30. Sutton, M.A.; Orteu, J.-J.; Schreier, H.W. *Image Correlation for Shape, Motion and Deformation Measurements—Basic Concepts, Theory and Applications*; Springer: Berlin, Germany, 2009; p. 317. [CrossRef]
31. Erbeck, R.; Merzkirch, W. Speckle photographic measurements of turbulence in an air stream with fluctuating temperature. *Exp. Fluids* **1988**, *6*, 89–93. [CrossRef]
32. Briers, J.D.; Webster, S. Quasi real-time digital version of single-exposure speckle photography for full-field monitoring of velocity or flow fields. *Opt. Commun.* **1995**, *116*, 36–42. [CrossRef]
33. Zuev, L.B.; Gorbatenko, V.V.; Pavlichev, K.V. Elaboration of speckle photography techniques for plastic flow analysis. *Measure Sci. Technol.* **2010**, *21*, 054014. [CrossRef]
34. Campbell, J.D.; Ferguson, W.G. The temperature and strain-rate dependence of the shear strength of mild steel. *Phil. Mag.* **1970**, *21*, 63–82. [CrossRef]
35. Lloyd, D.; Court, S.A.; Gatenby, K.M. Lüders elongation in Al-Mg alloy AA5182. *Mater. Sci. Technol.* **1997**, *13*, 660–666. [CrossRef]

36. Jin, H.; Lloyd, D.J. Effect of a duplex grain size on the tensile ductility of an ultra-fine grained Al-Mg alloy, AA5754, produced by asymmetric rolling and annealing. *Scr. Mater.* **2004**, *50*, 1319–1323. [CrossRef]
37. Cai, Y.L.; Yang, S.L.; Fu, S.H.; Zhang, Q.C. The influence of specimen thickness on the Lüders effect of a 5456 Al-based alloy: Experimental observations. *Metals* **2016**, *6*, 120. [CrossRef]
38. Danilov, V.I.; Gorbatenko, V.V.; Danilova, L.V.; Orlova, D.V. Features of localized plasticity autowaves in an FCC-alloy. *Russ. Phys. J.* **2021**, *64*, 397–403. [CrossRef]
39. Estrin, Y.; Kubin, L.P. Collective dislocation behaviour in dilute alloys and the Portevin—Le Chatelier effect. *J. Mech. Behavior Mater.* **1989**, *2*, 255–292. [CrossRef]
40. Mikhailov, A.S.; Loskutov, A.Y. *Foundations of Synergetics II*; Springer: Berlin/Heidelberg, Germany, 1991; p. 212. [CrossRef]
41. McCormick, P.G. A model for Portevin-Le Chatelier effect in substitutional alloys. *Acta Met.* **1972**, *20*, 351–354. [CrossRef]
42. Wert, G. *Modern Research Techniques in Physical Metallurgy*; American Society for Metals: Cleveland, OH, USA, 1952; p. 335.